

High sensitivity SPR refractive index sensor with high resolution based on anti-resonance fiber*

ZHANG Ailing**, LI Yueting, PAN Fei, PAN Honggang, and LIU Fei

Engineering Research Center of Optoelectronic Devices & Communication Technology, Ministry of Education, Tianjin Key Laboratory of Film Electronic and Communication Devices, School of Integrated Circuit Science and Engineering, Tianjin University of Technology, Tianjin 300384, China

(Received 15 June 2021; Revised 11 August 2021)

©Tianjin University of Technology 2022

We proposed a surface plasmon resonance (SPR) refractive index sensor based on hollow-core anti-resonance fiber (HC-ARF). Gold was filled in two symmetric cladding tubes of the fiber, while the analyte was filled in central air holes. The sensing performance was investigated by the finite element method (FEM). Results show that two resonance peaks (a crossing point around 1 030 nm and an anti-crossing region around 1 065 nm) appear for *x*-polarization (*x*-pol) core mode coupling with the surface plasmon polariton (SPP) mode. Moreover, the sensitivity was also analyzed. The sensitivity increased with the increase of cladding tube thickness *t*. The sensor with thickness *t*=1.7 μm gave a wavelength sensitivity of 7 350—14 790 nm/RIU in the refractive index range of 1.33—1.45 with resonance wavelength from 1 900 nm to 450 nm. Meanwhile, the resolution of 10⁻⁶ RIU was achieved. Thanks to high sensitivity and resolution, the proposed sensor has potential applications in glucose detection.

Document code: A **Article ID:** 1673-1905(2022)04-0204-6

DOI <https://doi.org/10.1007/s11801-022-1097-7>

Hollow-core anti-resonance fiber (HC-ARF)^[1], composed of several cladding air tubes and one central air hole, mainly restricts light in the central hole based on anti-resonance mechanism^[2]. It has important applications in refractive index sensing due to advantages of low transmission loss and simple structure. Recently, MENG^[3] designed a refractive index sensor by filling all air areas of HC-ARF with analyte liquid and sensitivity of 2 932 nm/RIU was obtained, which indicated that HC-ARF has potential applications in refractive index sensing, especially for liquids. According to the principle of surface plasmon resonance (SPR)^[4,5], various SPR refractive index sensors based on photonic crystal fibers (PCFs) with improved sensitivity have attracted much attention. In 2019, an SPR sensor based on symmetrical side-polished dual-core photonic crystal fiber (DC-PCF) was analyzed^[6]. Numerical simulation results showed a maximum sensitivity as high as 8 000 nm/RIU for the analyte refractive index of 1.42.

However, sensitivity larger than 10 000 nm/RIU is required in chemical and biological detection. In 2020, an SPR sensor adopting four-core PCF with high sensitivity up to 14 000 nm/RIU was designed^[7]. Later, an SPR sensor based on D-shaped PCF with wavelength sensitivity of 12 600 nm/RIU was proposed^[8]. Compared with PCF, HC-ARF has a completely different light guiding mechanism. In 2020, a hollow-core negative curvature fiber with high birefringence was proposed for low re-

fractive index sensing based on surface plasmon resonance effect^[9]. The sensing performances in the low refractive index range of 1.20—1.34 are evaluated by the traditional confinement loss method and the maximum sensitivity is up to 6 100 nm/RIU. In order to explore more sensitive sensors, a refractive index sensor that combines HC-ARF with SPR is investigated in this paper. Results show that the SPR sensor based on HC-ARF has high sensitivity and resolution.

The structure of the sensor based on HC-ARF is shown in Fig.1. According to the HC-ARF from Ref.[10], it has eight cladding tubes and a large core with radius *R*=24 μm, which refers to the shortest distance from the center of the fiber to the outer surface of the cladding tubes. The refractive index of the fiber *n*₁ is described by Sellmeier formula^[11]

$$n_1 = \sqrt{1 + B_1^2 / (\lambda^2 - C_1) + B_2^2 / (\lambda^2 - C_2) + B_3^2 / (\lambda^2 - C_3)}, \quad (1)$$

where *B*₁=0.691 663, *B*₂=0.407 943, *B*₃=0.897 479, *C*₁=0.004 679, *C*₂=0.013 512 and *C*₃=97.934 003. *λ* is the wavelength of free space. Three structures, single hole filling, two opposing holes filling and full filling, are analyzed in simulation. For full filling, the coupling bandwidths of surface plasmon polariton (SPP) mode and core-guided mode are too wide. So it is not suitable for sensing detection. In the comparison of single-hole

* This work has been supported by the Key Project of Tianjin Natural Science Foundation (No.20JCZDJC00500).

** E-mail: alzhang@email.tjut.edu.cn

and two-hole filling, it is found that the sensitivity of single-hole filling is lower than that of two-holes. So two opposing holes are selected for filling. Two symmetrical air tubes are filled with gold. The dielectric constant of gold is described by the Drude-Lorentz model^[12]. The analyte is filled in the large core of the fiber and its refractive index is represented by n . SPR phenomenon is analyzed by the finite element method (FEM). In FEM analysis, the free triangle mesh is selected. The real and imaginary parts of the effective refractive index are calculated through mode analysis to analyze dispersion and confinement loss. In order to investigate single-mode propagation of HC-ARF, the figure of mode (FOM_{11})^[13] is used to analyze the higher-order mode rejection ratio of ARF. It is expressed as

$$FOM_{11} = \alpha_{11} / \alpha_{01} - 1, \quad (2)$$

where α_{01} is the loss of LP₀₁ core-guided mode and α_{11} is the loss of LP₁₁ core-guided mode.

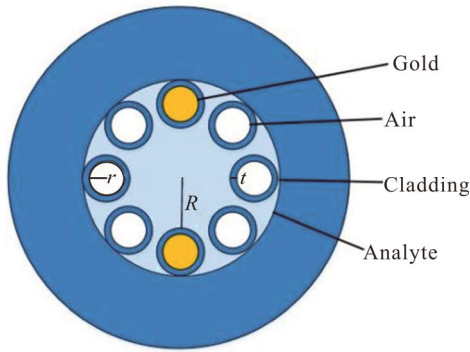


Fig.1 Structure of HC-ARF and sensor filled with gold in two symmetrical air tubes

The radius and thickness of cladding tubes are represented by r and t , respectively. FOM_{11} of HC-ARF versus r/R is shown in Fig.2 under the condition of $t=0.48 \mu\text{m}$, $n=1.34$ and $\lambda=1550 \text{ nm}$. When $r/R=0.48$, the loss of higher-order mode is much larger than the loss of LP₀₁ core mode. Moreover, the $FOMs$ of HC-ARF corresponding to different operating wavelengths have also been analyzed and the most optimized values of r/R with different wavelengths are shown in Fig.2. It is clear that as the wavelength increases, the value of r/R gradually increases. Meanwhile, when gold and analyte are filled, the sensor only supports LP₀₁ mode transmission no matter how r/R changes, and it is the same for different wavelengths. So r is set to $11.52 \mu\text{m}$ in the following analysis, which can meet the single-mode transmission condition of the optical fiber without affecting the sensor.

SPR phenomena for both x -polarization (x -pol) and y -polarization (y -pol) electric fields are analyzed at wavelengths from 600 nm to 1800 nm . We find that only the x -pol core mode can be coupled with the SPP mode, while the coupling between y -pol core mode and SPP mode is not found in this wavelength range. The dispersions of x -pol core mode and SPP mode are achieved

from the real part of corresponding mode effective refractive index with analyte refractive index at 1.34 , which is shown in Fig.3(a). From the figure, the dispersions show a crossing point around 1030 nm and an anti-crossing region around 1065 nm .

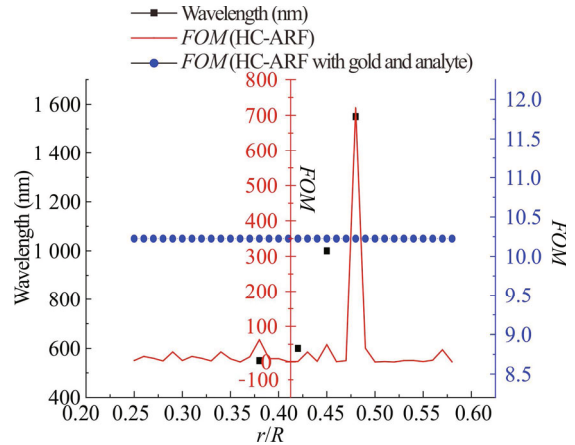


Fig.2 FOM_{11} of HC-ARF with $R=24 \mu\text{m}$, $t=0.48 \mu\text{m}$, $n=1.34$, and $\lambda=1550 \text{ nm}$

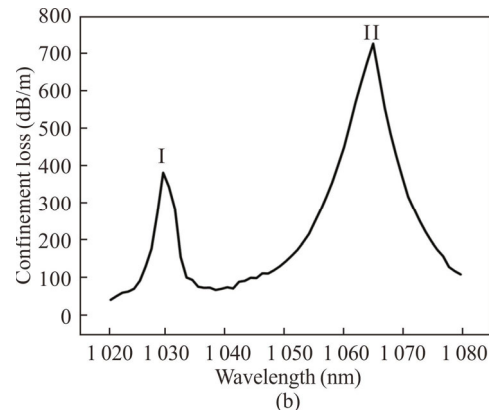
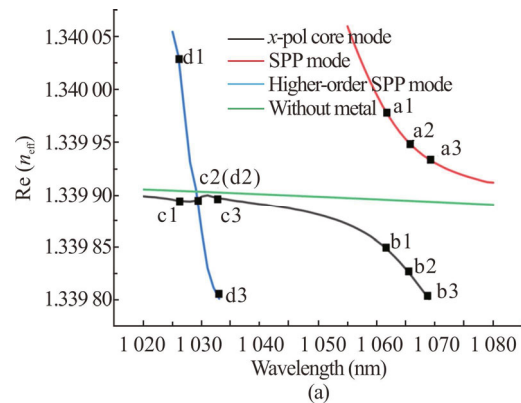


Fig.3 (a) $\text{Re}(n_{\text{eff}})$ of the x -pol core mode and various SPP modes when $n=1.34$; (b) Confinement loss of SPP-coupled core mode with wavelength for $n=1.34$ when $R=24 \mu\text{m}$, $r=11.52 \mu\text{m}$, and $t=0.48 \mu\text{m}$

Confinement loss is used to describe the confinement ability of the fiber core to light. It is achieved from the

imaginary part of core-guided mode effective index, which is expressed as^[14]

$$\alpha_{\text{loss}} \text{ (dB/m)} = -8.86 \cdot k_0 \text{ Im}[n_{\text{eff}}], \quad (3)$$

where $k_0=2\pi/\lambda$ is the propagation constant corresponding to the incident wavelength and $\text{Im}[n_{\text{eff}}]$ represents the imaginary part of the core-guided mode effective refractive index. The confinement loss of SPP-coupled core mode is shown in Fig.3(b). A weaker peak (I) and an apparent peak (II) are observed at the resonance wavelength, which indicates maximum energy transfers from the core-guided mode to the SPP mode.

The electric field distributions of the *x*-pol core mode and SPP mode near the anti-crossing region are shown in Fig.4. Obviously, in the anti-crossing region, the electric fields of the *x*-pol core mode and the SPP mode exchange. It can be seen from Fig.4(b) and Fig.4(e) that more energy transfers from the core to the SPP mode. The electric field distributions of the core mode and the SPP mode near peak I are illustrated in Fig.5. The phenomenon in Fig.5(b) indicates that the 3rd-order SPP mode is coupled with the core mode. More energy transfers from the core mode to the 3rd-order SPP mode and a weaker loss peak (I) appears at point c2. It is discovered that the 2nd-order SPP mode appears at longer wavelength in Fig.5(c).

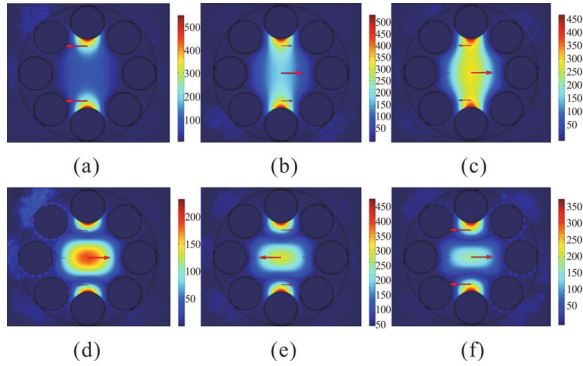


Fig.4 Electric field distributions of the core mode and SPP modes near the anti-crossing point: (a) a1, (b) a2, (c) a3, (d) b1, (e) b2, and (f) b3 corresponding to those in Fig.3(b)

The sensitivity can be obtained from the following equation

$$S = d\lambda / dn, \quad (4)$$

where $d\lambda$ is the change of the resonance wavelength and dn is the change of analytes refractive index. The sensitivity is also investigated and results show that sensitivity of peak I is slightly lower than that of peak II. So, the influence of R , r and t on the sensitivity of peak II is discussed in the following part.

The sensor sensitivities corresponding to different $R(r)$ are respectively analyzed around $n=1.34$ with other structure parameters constant, as shown in Fig.6. As R increases, the sensitivity first increases and then de-

creases, and so does r . But overall, both R and r have less influence on the sensitivity. In the following analysis, it is reasonable to set $R=24 \mu\text{m}$ and $r=11.52 \mu\text{m}$ where the sensor achieved maximum sensitivity.

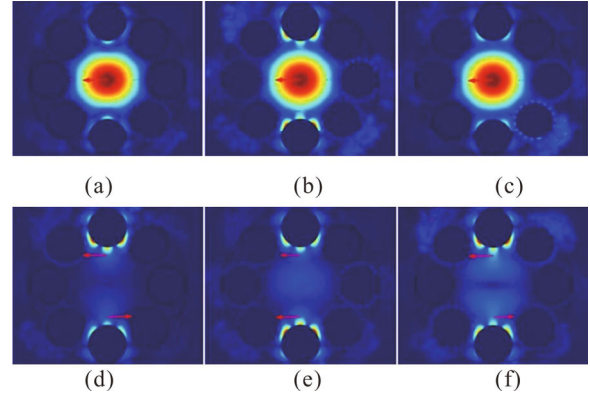


Fig.5 Electric field distributions of the core mode and SPP modes near the crossing point: (a) c1, (b) c2, (c) c3, (d) d1, (e) d2, and (f) d3 corresponding to those in Fig.3(b)

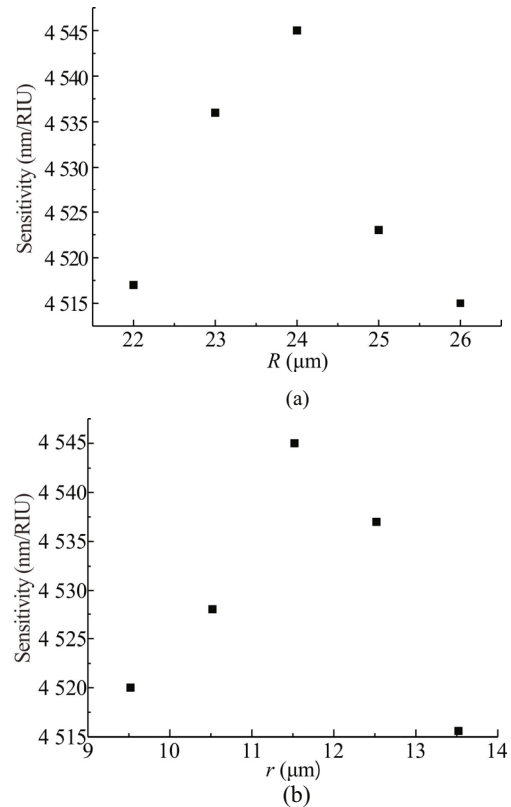


Fig.6 Sensor sensitivities around $n=1.34$ versus (a) R with $r=11.52 \mu\text{m}$ and $t=0.48 \mu\text{m}$, and (b) r with $R=24 \mu\text{m}$ and $t=0.48 \mu\text{m}$

According to the light guiding mechanism of HC-ARF, only when the anti-resonance condition is met, the light transmission is limited in the core. The effective refractive index of core mode with different t in the range of 0.4—3.35 μm is analyzed as shown in Fig.7.

The maximum value of t ($3.35 \mu\text{m}$) is obtained when eight cladding air tubes contact to each other. The inset (b) in Fig.7 implies that light cannot be confined in the core of fiber near $t=0.8 \mu\text{m}$. Core mode is guided in HC-ARF with t in the range of $t < 0.76 \mu\text{m}$ and $0.82 \mu\text{m} < t < 3.35 \mu\text{m}$. In addition, the result also shows that the thickness t selected in the previous analysis satisfies the anti-resonance condition. The observed SPR phenomenon is indeed caused by the coupling of the core mode and SPP mode.

The sensitivities of peak II corresponding to different t around $n=1.34$ are also shown in Fig.7. Obviously, in the two guiding mode regions, the sensitivity increases approximately linearly with thickness t increasing. The sensitivity in the region of $t > 1.5 \mu\text{m}$ is higher than that of $t < 0.76 \mu\text{m}$. When the thickness t is $3.35 \mu\text{m}$, maximum sensitivity of $13\,500 \text{ nm/RIU}$ can be achieved around $n=1.34$. However, the resonance wavelength is larger than $2 \mu\text{m}$.

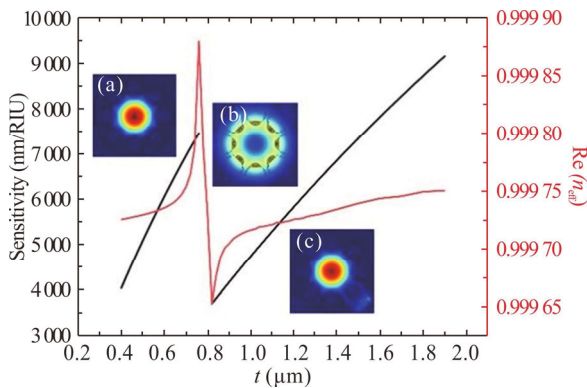


Fig.7 Effective refractive index of the x-pol core mode and the sensor sensitivity with $n=1.34$ and $t=0.4\text{—}3.35 \mu\text{m}$

Therefore, considering the position of resonance wavelength, the resonance wavelength versus refractive index of analytes with $n=1.33\text{—}1.45$ for $t=1.5 \mu\text{m}$ and $1.7 \mu\text{m}$ are analyzed, which is shown in Fig.8. For constant thickness t , the resonance wavelength gradually blue shifts and the sensing sensitivity gradually increases with the analyte refractive index increasing. When the thickness t is $1.7 \mu\text{m}$, the sensing sensitivity can reach $14\,790 \text{ nm/RIU}$ for an analyte refractive around 1.45 and $7\,350 \text{ nm/RIU}$ around 1.33 . And the confinement loss with $t=1.7 \mu\text{m}$ is shown in Fig.9. It can be confirmed that as the refractive index increases, the resonance peak gradually blue shifts.

The sensor resolution can be found from the following equation^[15]

$$R(\text{RIU}) = \Delta\lambda_{\min} / S, \quad (5)$$

where $\Delta\lambda_{\min}$ is the minimum spectral resolution. High blood glucose levels can lead to diabetes and low blood glucose levels can lead to hypoglycemia. The refractive index of glucose solution can be calculated by^[5]

$$n_c = 0.000\,118\,89c + 1.332\,305\,45, \quad (6)$$

where n_c is the glucose solution refractive index and c is the glucose concentration.

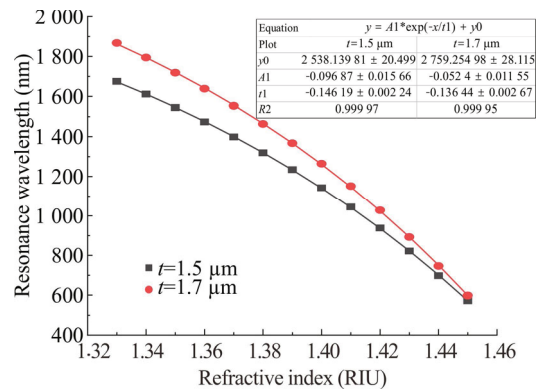


Fig.8 SPR resonance wavelength versus analyte refractive index ($1.33 < n < 1.45$) when $t=1.5 \mu\text{m}$ and $1.7 \mu\text{m}$

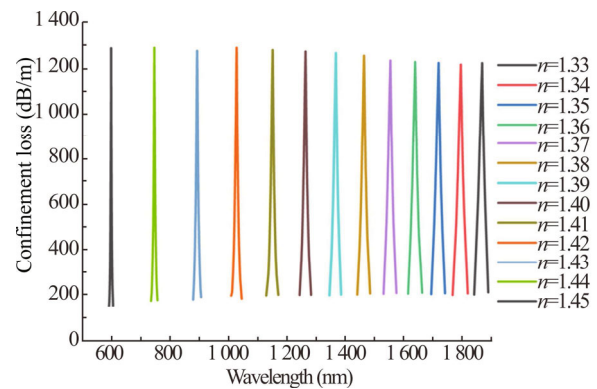


Fig.9 Confinement loss versus wavelength ($1.33 < n < 1.45$) when $t=1.7 \mu\text{m}$

Normal blood glucose has refractive index around $1.332\,3\text{—}1.332\,4$ and concentration of $0.70\text{—}1.40 \text{ g/L}$. The confinement loss for $n=1.332\,3$ and $1.332\,4$ are shown in Fig.10. Peak I and peak II both can be observed in two cases. And it is observed that the electric field distribution near the two resonance points is similar to that in Fig.3. At peak I, when the refractive index changes from $1.332\,3$ to $1.332\,4$, the resonance wavelength changes from $1\,805.1 \text{ nm}$ to $1\,803.4 \text{ nm}$. At peak II, when the refractive index changes from $1.332\,3$ to $1.332\,4$, the resonance wavelength changes from $1\,849.8 \text{ nm}$ to $1\,847.9 \text{ nm}$. Therefore, the sensitivity of peak I is $15\,000 \text{ nm/RIU}$ while the sensitivity of peak II is $19\,000 \text{ nm/RIU}$. It is confirmed that the sensitivity of peak I is lower than that of peak II. Moreover, the drift range of peak II is larger than that of peak I. It is obvious that when peak II is used for detection, there will be no influence on peak I. When the concentration changes by 0.10 g/L , the refractive index changes by 10^{-6} RIU . So, in order to measure glucose concentration smaller than 0.10 g/L , the sensing resolution is required to reach 10^{-6} RIU . According to the minimum spectral resolution corresponding to different spectrometers, the sensor resolution for an analyte refractive around 1.33 can be

obtained, as shown in Tab.1. When wavelength resolution of the instrument is 0.02 nm, 0.05 nm and 0.07 nm, the sensor with a resolution of 10^{-6} RIU is achieved, which is efficient for human glucose detection. Therefore, the sensor proposed in this paper is useful for glucose detection.

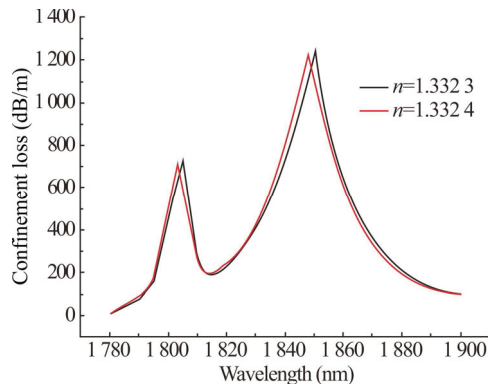


Fig.10 Confinement loss of SPP-coupled core mode versus wavelength for $n=1.3323$ and 1.3324 when $R=24 \mu\text{m}$, $r=11.52 \mu\text{m}$, $t=1.7 \mu\text{m}$

Tab.1 Sensor resolutions around $n=1.33$ with different minimum spectral resolutions when $t=1.7 \mu\text{m}$

Minimum spectral resolution (nm)	Sensor resolution (10^{-6} RIU)
0.02	2.72
0.05	6.80
0.07	9.52
0.1	13.61
0.5	68.03

Tab.2 Comparison of other PCF-based and HC-ARF-based SPR sensors performances

Sensor type	Refractive index range (RIU)	Maximum sensitivity (nm/RIU)	Reference
Dual-core DC-PCF	1.30—1.42	8 000	[6]
D-shaped PCF	1.15—1.36	12 600	[7]
HC-ARF filled with analyte in all holes	1.20—1.40	2 932	[3]
HC-ARF with high birefringence	1.20—1.34	6 100	[9]
This work	1.33—1.45	14 790	

In this paper, an SPR refractive index sensor based on eight-tube hollow core anti-resonance fiber with high sensitivity and resolution is designed. The central air hole is used as an analyte channel. Gold is filled in two symmetric

cladding tubes. The cladding core aperture and cladding tube thickness of the anti-resonance fiber are determined by FEM. In conclusion, we can improve the sensing sensitivity by increasing the thickness of cladding tubes. When the thickness is $1.7 \mu\text{m}$, the sensing sensitivity can reach $14\,790 \text{ nm/RIU}$ for an analyte refractive around 1.45, which is better than result in Ref.[7]. Meanwhile, the sensing sensitivity can reach $7\,350 \text{ nm/RIU}$ and the resolution can be 10^{-6} RIU for an analyte refractive around 1.33, which is efficient for human glucose detection. In addition, the experiment of filling the nanowire solution into PCF has been successfully realized in Ref.[5]. So, the sensor designed in this paper is feasible. Therefore, the sensor has potential applications for detection of glucose and has a good application prospect for the diagnosis and treatment of diabetes.

Statements and Declarations

The authors declare that there are no conflicts of interest related to this article.

References

- [1] MOUSAVI S A, SANDOGHCHI S R, RICHARDSON D J, et al. Broadband high birefringence and polarizing hollow core antiresonant fibers[J]. Optics express, 2016, 24(20): 22943-22958.
- [2] YU F, KNIGHT J C. Negative curvature hollow-core optical fiber[J]. IEEE journal of selected topics in quantum electronics, 2016, 22(2): 146-155.
- [3] MENG F C. Study on transmission characteristics and related sensors of hollow core negative curvature fiber[D]. Qinhuangdao: Yanshan University, 2019: 48-53. (in Chinese)
- [4] PATHAK A K, SINGH V K. SPR based optical fiber refractive index sensor using silver nanowire assisted CSMFC[J]. IEEE photonics technology letters, 2020, 32(8): 465-468.
- [5] YANG X C, LU Y, WANG M T, et al. A photonic crystal fiber glucose sensor filled with silver nanowires[J]. Optics communications, 2016, 359(21): 279-284.
- [6] WANG S, LI S G. Surface plasmon resonance sensor based on symmetrical side-polished dual-core photonic crystal fiber[J]. Optical fiber technology, 2019, 51(3): 96-100.
- [7] LIAO J F, DING Z P, XIE Y M, et al. Ultra-broadband and highly sensitive surface plasmon resonance sensor based on four-core photonic crystal fibers[J]. Optical fiber technology, 2020, 60(5): 102316.
- [8] ZENG W Y, WANG Q L, XU L. Plasmonic refractive index sensor based on D-shaped photonic crystal fiber for wider range of refractive index detection[J]. Optik, 2020, 223(11): 165463.
- [9] QIU S, YUAN J, ZHOU X, et al. Hollow-core negative curvature fiber with high birefringence for low refractive index sensing based on surface plasmon resonance

- effect[J]. *Sensors*, 2020, 20(22): 6539.
- [10] PRYAMIKOV A, ALAGASHEV G, FALKOVICH G, et al. Light transport and vortex-supported wave-guiding in micro-structured optical fibres[J]. *Scientific reports*, 2020, 10(1): 2507.
- [11] FAN Z K, LI S G, LIU Q, et al. High sensitivity of refractive index sensor based on analyte-filled photonic crystal fiber with surface plasmon resonance[J]. *IEEE photonics journal*, 2015, 7(3): 1-9.
- [12] ZONG C J, ZHANG D. Analysis of propagation characteristics along an array of silver nanorods using dielectric constants from experimental data and the Drude-Lorentz model[J]. *Electronics*, 2019, 8(11): 1280.
- [13] UEBEL P, GÜNENDI M C, FROSZ M H, et al. Broadband robustly single-mode hollow-core PCF by resonant filtering of higher-order modes[J]. *Optics letters*, 2016, 41(9): 1961-1964.
- [14] HAXHA S, ADEMGIL H. Novel design of photonic crystal fibres with low confinement losses, nearly zero ultra-flatted chromatic dispersion, negative chromatic dispersion and improved effective mode area[J]. *Optics communications*, 2008, 281(2): 278-286.
- [15] RIFAT A A, MAHDIRAJI G A, SUA Y M, et al. Highly sensitive multi-core flat fiber surface plasmon resonance refractive index sensor[J]. *Optics express*, 2016, 24(3): 2485-2495.